Appl Phys A (2011) 105:795–800
DOI 10.1007/s00339-011-6651-2

Applied Physics A
Materials Science & Processing

RAPID COMMUNICATION

The effects of a thin film dopant precursor on the structure and properties of femtosecond-laser irradiated silicon

Matthew J. Smith · Mark Winkler · Meng-Ju Sher · Yu-Ting Lin · Eric Mazur · Silvija Gradečak

Received: 20 July 2011 / Accepted: 10 October 2011 / Published online: 28 October 2011

Abstract Femtosecond (fs) laser irradiation of a silicon substrate coated with a thin film is a flexible approach to producing metastable alloys with unique properties, including near-unity sub-band gap absorptance extending into the infrared. However, dopant incorporation from a thin film during fs-laser irradiation is not well understood. We study the thin film femtosecond-laser doping process through optical and structural characterization of silicon fs-laser doped using a selenium thin film, and compare the resulting microstructure and dopant distribution to fs-laser doping with sulfur from a gaseous precursor. We show that a thin film dopant precursor significantly changes the laser-material interactions, modifying both the surface structuring and dopant incorporation processes and in turn affecting p–n diode behavior.

1 Introduction

Silicon-based optoelectronic devices that operate at photon energies less than the band gap (1.1 eV) are of great interest for infrared detectors and silicon-based photovoltaics. Ultrafast laser irradiation of silicon [1] can be used to introduce chalcogens concentrations in Si up to 10^{19}–10^{20} cm^{-3}, several orders of magnitude beyond their equilibrium solid solubility limit (10^{16}–10^{17} cm^{-3}) [2, 3]. Such hyperdoped silicon exhibits unique near-unity sub-band gap absorptance down to photon energies less than 0.5 eV [4–7]. Notably, similar properties cannot be achieved through equilibrium material synthesis methods.

So far, non-equilibrium chalcogen concentrations have been successfully introduced into Si as a gas during fs-laser irradiation [4, 7, 8] and as a powder or thin film on the substrate prior to fs-irradiation [6, 7]. Low-bias Si photodiodes with responsivity to photon energies as low as 0.8 eV have been demonstrated based on Si hyperdoped using fs-laser irradiation in the presence of SF_6 gas [9]. To move the hyperdoping concept further, the deposition of a thin film of dopant on the substrate would enable the introduction of dopants that are unavailable, highly volatile, or toxic in the gas phase, and thus open up fs-laser doping to a wider range of elements [6, 7]. However, the extent to which fs-laser doping can be used to modify the band structure of silicon has been limited by a lack of understanding of the dopant incorporation process and resulting microstructure when using a thin film dopant precursor. A better understanding of thin film laser doping would therefore extend fs-laser doping as a platform technology for novel materials synthesis.

In this work, we investigate thin film fs-laser doping through the optical, structural, and electronic characterization of Si fs-laser doped using a thin film dopant precursor and compare the results to Si films doped using a gaseous precursor. Under identical irradiation conditions, fs-laser doping with a thin-film yields higher sub-band gap absorptance than doping with a gaseous precursor. Structural investigations show that a thin film dopant precursor strongly influences the surface structuring and dopant incorporation processes compared to doping with a gas-phase

M.J. Smith · S. Gradečak (✉)
Department of Materials Science and Engineering, Massachusetts Institute of Technology, Cambridge, MA 02139, USA
e-mail: gradecak@mit.edu
Fax: +1-617-258-7620

M. Winkler · M.-J. Sher · E. Mazur
Department of Physics, Harvard University, Cambridge, MA 02138, USA

Y.-T. Lin · E. Mazur
School of Engineering and Applied Sciences, Harvard University, Cambridge, MA 02138, USA

Table 1 Notation and corresponding fs-laser doping parameters for samples used in this study

Name	Dopant precursor	Fluence (kJ/m^2)	Shots per area (s/A)	Atmosphere (6.7×10^4 Pa)	Substrate Si(100)
Se:Si-1	Se thin film	4	88	N_2	n-Type (3000–6000 Ω cm)
SF_6:Si-1	SF_6 gas	4	88	SF_6	n-Type (3000–6000 Ω cm)
N_2:Si-1	None	4	88	N_2	n-Type (3000–6000 Ω cm)
Se:Si-2	Se thin film	4	88	N_2	p-Type (1–20 Ω cm)
SF_6:Si-2	SF_6 gas	8	50	SF_6	p-Type (1–20 Ω cm)

precursor, which has notable consequences on the resulting surface morphology, microstructure, and dopant distribution. We also discuss the impact of a thin-film fs-laser doping on p–n diode behavior due to the differences in microstructure and dopant distribution that arise from the use of a thin film precursor.

2 Methods

The Si samples were irradiated with above-ablation threshold Ti:sapphire fs-laser pulses (800-nm wavelength, 80-fs pulse duration) with a fluence of 4 kJ/m^2 and 88 shots per area (s/a). The detailed fs-laser doping procedure and experimental set-up have been described previously [7], and complete irradiation parameters used in this work are reported in Table 1. For thin film fs-laser doping, a 75 nm film of Se was deposited onto the silicon wafer prior to irradiation in nitrogen. To understand the effect of the thin film on the hyperdoping process, silicon was also irradiated in the presence of SF_6 gas, and in nitrogen without a dopant precursor. After laser exposure, the transmittance and reflectance of each sample was measured independently with a UV-Vis-NIR spectrophotometer equipped with an integrating sphere; from these spectra the absorptance ($A = 1 - T - R$) was calculated. The sample morphology was investigated using a FEI Helios 600 scanning electron microscope (SEM) operated at 5 kV accelerating voltage. Cross-sectional transmission electron microscopy (TEM) samples were prepared using a tripod polisher followed by a brief Ar^+-ion mill. Bright-field (BF) TEM micrographs and selected area diffraction patterns (SAD) were collected with a JEOL 2011 TEM operated at 200 kV. Dark-field scanning TEM (DF-STEM) and energy dispersive X-ray spectroscopy (EDX) were carried out on a JEOL 2010F TEM operated at 200 kV. To form p–n diodes, samples were annealed at 975 K for 30 minutes prior to patterning aluminum contacts using electron beam deposition.

3 Results and discussion

First, we compare the optical properties of samples prepared using thin film or gas precursors, as defined in Table 1. Figure 1(a) shows the absorptance of as-prepared fs-laser doped samples. All hyperdoped samples exhibit unique sub-band gap absorptance, but sample Se:Si-1 (prepared using a thin film precursor) has a higher average IR-absorptance (90%) than sample SF_6:Si-1 (70%), which was irradiated under the same conditions but in a presence of a gaseous precursor. Both samples have significantly greater IR absorptance than sample N_2:Si-1, which exhibits lower, monotonically decreasing absorptance in this spectral region, likely due to defect states induced by irradiation [7]. The difference in optical absorptance between the thin film-doped (Se:Si-1) and gas-phase doped (SF_6:Si-1) samples irradiated under identical conditions suggests that the doping process is strongly influenced by the phase of the dopant precursor. To achieve comparable absorptance for electronic characterization of samples prepared using different dopant precursors (discussed below), we prepared sample SF_6:Si-2 by increasing the laser fluence to 8 kJ/m^2 and used 50 s/A, which resulted in an average IR-absorptance of 84%.

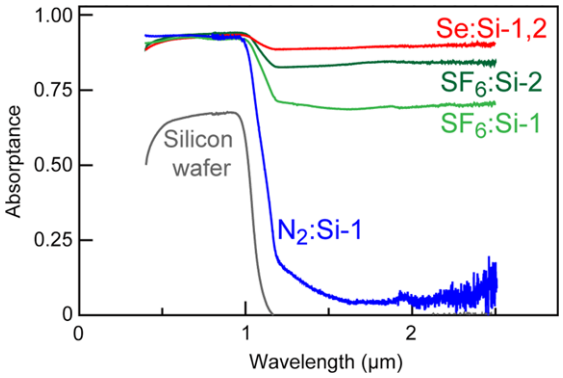

Fig. 1 Absorptance spectra of all samples presented in this work

To better understand the difference in irradiation conditions necessary to achieve high IR-absorptance for gas and thin film precursors, we investigated the morphology, microstructure, and dopant distribution using electron microscopy. The effect of the thin film on the surface microstructure was studied by comparing samples irradiated under identical conditions in an N_2 ambient, and with and without a Se thin film (samples Se:Si-1 and N_2:Si-1). We also gain insight into the unique aspects of the dopant incorporation resulting from the thin film doping by com-

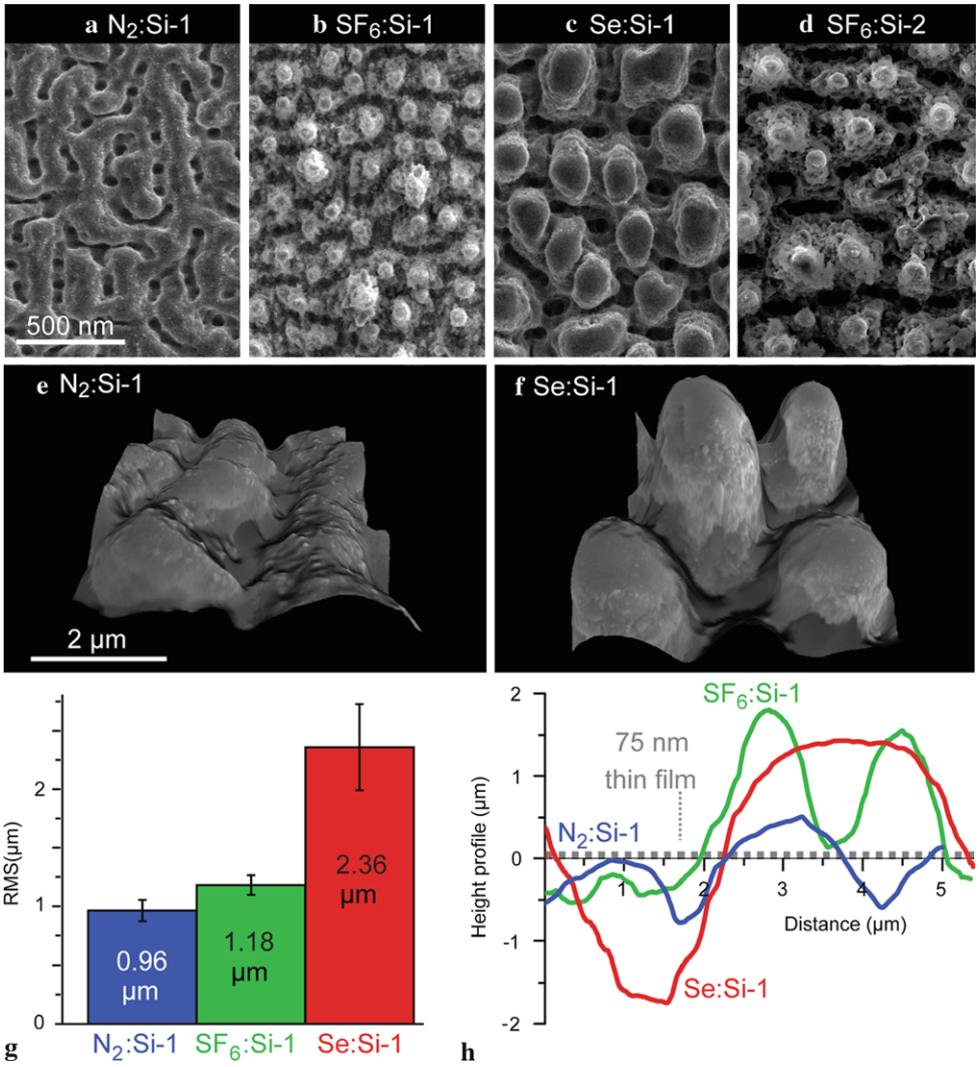

Fig. 2 (**a**–**d**) SEM micrographs showing surface morphology of fs-laser irradiated Si. The laser scan direction and polarization was in the horizontal direction. The same scale bar for all images. (**e**–**g**) Stereoscopically reconstructed 3D models of surfaces (**e**, **f**), used to extract the RMS of the surface height shown in (**g**). *Scale bar* in (**e**, **f**) reflects 2 µm along the front edge of the model. *Error bars* in RMS measurements reflect standard deviation for five independent measurements. (**h**) Height profiles of representative surface peaks and the relative thickness of the 75 nm Se film (*dashed*)

paring Se:Si-1 to SF_6:Si-1 and SF_6:Si-2. SEM images in Figs. 2(a)–2(d) show that all of the samples, regardless of the processing conditions, develop micrometer-scale periodic peaks through repeated melting and ablation of Si, but the size and shape of the spikes is strongly influenced by the dopant precursor phase. Notably, such surface structuring of silicon using fs-laser irradiation has been investigated as a process for creating antireflection and light-trapping surfaces for photovoltaics [1], but the effect of a thin film on the surface structuring process has not been explored. We quantified roughness of the surface by measuring the root-mean-square (RMS) of the height from stereoscopically reconstructed models [10] of SEM images taken at 0°, −10°, and +10° tilts (Figs. 2(e), 2(f)). The presence of the 75 nm film of Se causes the RMS to increase by over 200%, from 0.96 µm for N_2:Si-1 to 2.36 µm for Se:Si-1 (Fig. 2(g)), an increase more than an order of magnitude larger than the initial Se film thickness indicated in Fig. 2(h)

From the change in amplitude related to the thin film dopant precursor, it is clear that the Se thin film significantly influences the laser-induced surface structuring process. To better understand the surface structuring and dopant incorporation processes, the samples were next investigated using cross-sectional TEM and EDX chemical analysis. BF-TEM images and corresponding SAD of N_2:Si-1 sample (Fig. 3(a)) demonstrate that a 100–300-nm thick surface layer is laser-modified when no dopant precursors are present, and the surface peaks retain the same crystalline orientation as the substrate, though occasionally a misoriented grain was identified (not shown). In both SF_6:Si samples a sulfur-rich layer was observed on the surface while the peaks retain a single-crystalline, undoped core, consistent with previous findings [11]. (The thickness of the S-doped layer changes with fluence, but it is generally less than 300 nm in both SF_6:Si samples.)

In contrast to other samples, thin film-doped samples exhibit a distinct dopant distribution and microstructure. As shown in Fig. 3(d), Se:Si-1 contains micrometer-scale volumes of polycrystalline Si within each surface peak, as confirmed by the corresponding SAD patterns. Using DF-

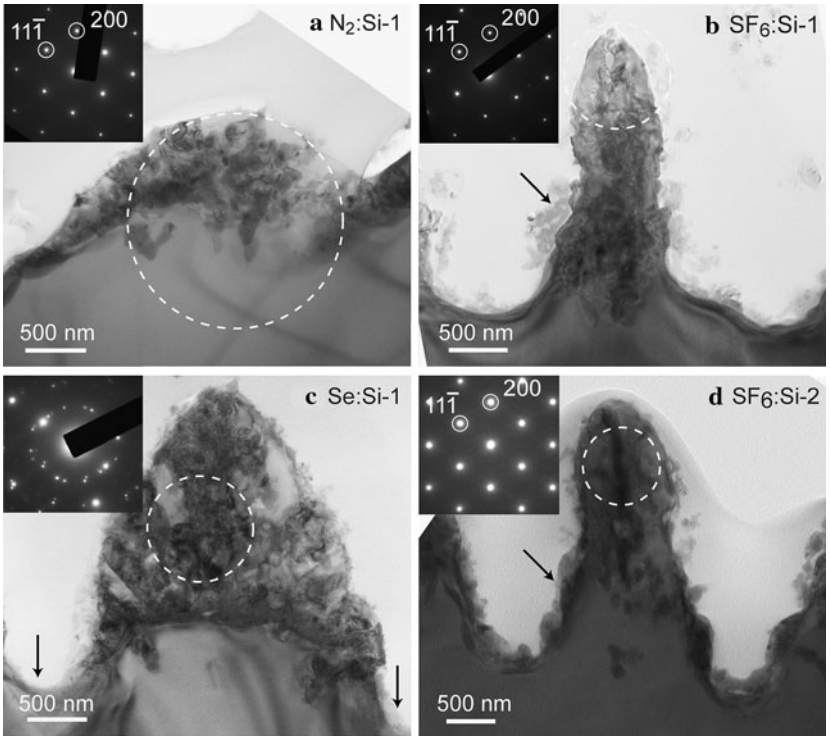

Fig. 3 Cross-sectional BF-TEM images taken along the Si [011] zone axis with corresponding selected area diffraction patterns (*insets*). *Black arrows* indicate selenium-free valleys in (**a**), and identify the sulfur-rich surface layer in (**c**–**d**). The observed BF-TEM contrast within the core of N_2:Si-1 and SF_6:Si peaks corresponds to pockets of amorphous material, as confirmed by convergent beam electron diffraction [17]

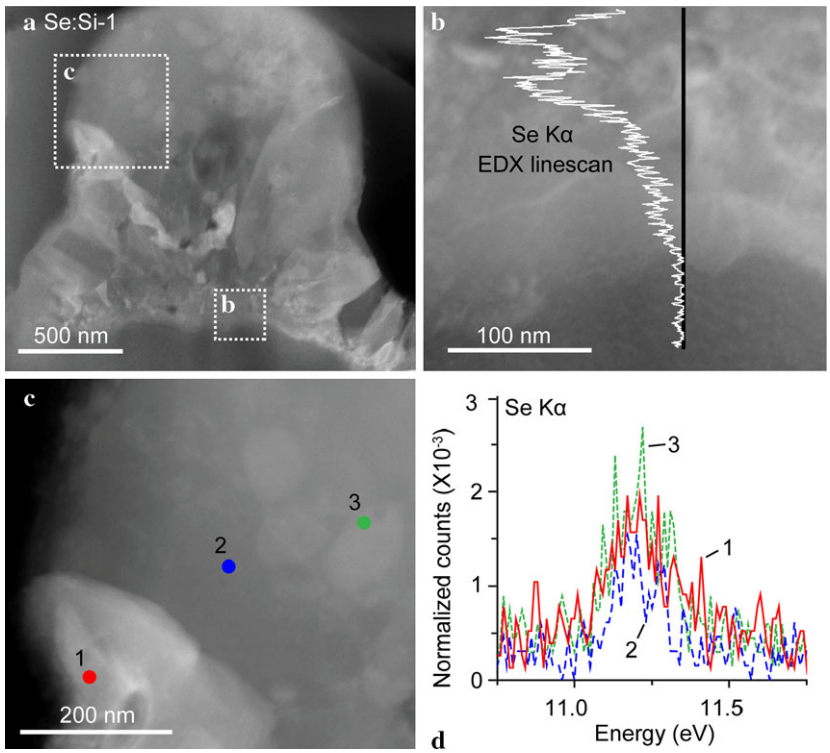

Fig. 4 (**a**) DF-STEM image of Se:Si-1, *dashed boxes* highlight the regions shown in (**b**) and (**c**). (**b**) Selenium EDX line scan across the doped-undoped interface. (**c**) DF-STEM image showing the location of SeK_α EDX point spectra shown in (**d**)

STEM and EDX (Fig. 4), we show that the *entire* polycrystalline region is Se-rich, as opposed to the surface-only doping of SF_6:Si samples. A series of EDX point scans and the corresponding SeK_α EDX peaks (Figs. 4(c)–4(d)) indicate that the Se concentration is on the order of 10^{19}–10^{20} cm^{-3} (0.1–1%). We note that here EDX can be used only qualitatively, as the measured concentrations are at the lower limit of the EDX chemical resolution. As shown in Fig. 4(b), an EDX line scan from the Si substrate into the polycrystalline doped region confirms that Se is incorporated throughout the

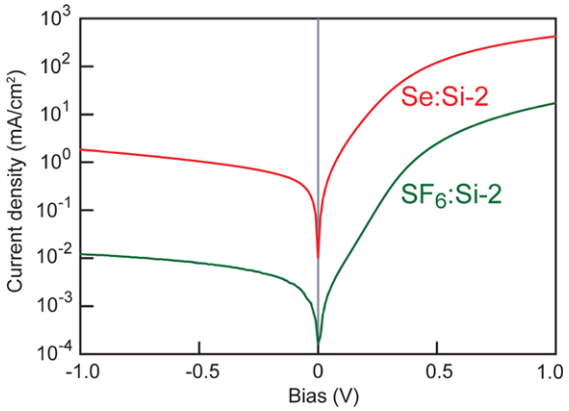

Fig. 5 Current density vs. bias curves of Se:Si-2 and SF_6:Si-2 at room temperature

entire polycrystalline region with some local variations in the Se composition.

The general structure of the control sample (N_2:Si-1) and sulfur-doped samples (SF_6:Si-1,2) is consistent with the current understanding of fs-laser induced surface structuring and dopant incorporation [12, 13]. During fs-laser irradiation above the ablation threshold, a thin layer of material (estimated to be approximately 100 nm for SF_6:Si samples) is ablated from the surface and a molten Si layer is left behind. When a gas is present during irradiation, it is atomized by the high intensity of the ultra-short laser pulse and mixes with the molten Si [14], which then resolidifies quickly due to its contact with the cold bulk substrate [15]. However, the morphology, microstructure, and dopant distribution in Se:Si-1 cannot be explained by the gas-phase doping model discussed above and together present a strong evidence that a thin film dopant precursor changes the surface structuring and dopant incorporation processes, as discussed below (Fig. 5).

The micrometer-scale volumes of the generated Se-doped material are an order of magnitude deeper than typical silicon melt depths under these conditions, and are likely the source of the strong sub-band gap absorptance observed in Se:Si-1 (90%) compared to SF_6:Si-1 (70%). The Se–Si and S–Si phase diagrams [16] show that substantial suppression of the chalcogen-silicon melt temperature is possible only when the chalcogen concentration is greater than 40–50 at%. During early-stage irradiation, a thin film of dopant precursor provides sufficiently high concentrations of chalcogens at the surface to suppress the melt temperature and thus increase the melt depth. On the other hand, when treated as an ideal gas, the concentration of S in SF_6 gas is about 2×10^{19} cm^{-3} under typical structuring conditions, which is less than 1% of the atomic density of silicon. The melt depths observed in N_2:Si-1 and SF_6:Si samples are similar and less than 300 nm (Figs. 3(a), 3(b), 3(d)), indicating that a gaseous dopant precursor does not provide sufficient concentrations to substantially suppress the melt temperature and thus increase the melt depth.

Although only ~1% Se was observed in the recrystallized region, we suggest that additional dopant redistribution occurs during later-stage laser irradiation. The lack of dopant in the "valleys" of the Se:Si-2 surface (Fig. 3(d), black arrows) is consistent with the finite source of Se available for incorporation. During later-stage irradiation, as material is ablated away from regions between the peaks, Se is lost from these regions without being replenished. Similar ablation processes occur during irradiation in SF_6, but sulfur is available for incorporation even during later-stage irradiation due to the steady supply of a gaseous precursor. The thin film of selenium, however, represents a finite resource for doping; the this film is either incorporated into silicon or ablated away during earlier-stage irradiation.

Finally, to investigate the consequences of thin-film fs-laser doping on p–n diode behavior, we fabricated SF_6-doped (SF_6:Si-2) and Se-doped (Se-:Si-2) samples on a p-type substrate. Fs-laser irradiation conditions were chosen for SF_6:Si-2 such that it exhibited similar optical properties to Se:Si-2, as shown in Fig. 1(a). The Se:Si-2 diode shows rectification (Fig. 5), confirming that the Se dopants act as donors and produce a junction with the p-type substrate. The Se:Si-2 diode (Fig. 5), however, exhibits a higher leakage current than the SF_6:Si-2 diode, which could be a consequence of the unique dopant distribution and microstructure arising from using a thin film precursor during the doping process.; the discontinuous nature of the thin film-doped Se:Si surface creates shunts at the p–n junction, whereas SF_6:Si has a continuous surface layer of doped material. Nevertheless, our results show that thin film doping is a valuable technique for synthesizing surfaces of hyperdoped silicon with sub-band gap absorption and can produce rectifying p–n diodes. Future studies will concentrate on using this understanding of the melting and ablation processes that occur during thin film fs-laser doping to tailor the surface structure and dopant distribution.

4 Conclusion

In summary, a thin film dopant precursor compared to a gas precursor changes both the surface structuring and dopant incorporation processes in fs-laser doped silicon. Thin film fs-laser doping generates larger volumes of doped material than doping from a gas and achieves higher sub-band gap absorptance at lower fluences. Both processes can yield rectifying p–n diodes, but future improvement of p–n diodes based on thin film dopants will require improvement of the discontinuous dopant distribution. The successful synthesis of novel hyperdoped materials for optoelectronic applications requires an in-depth understanding of the modified surface structuring and dopant incorporation processes, which

will enable more rational control of the resulting microstructure and dopant distribution. This work represents progress in understanding thin film fs-laser doping as an inexpensive, flexible, and unique platform for novel materials synthesis.

Acknowledgements We thank Professor Tonio Buonassisi, Professor Mike Aziz, Joe Sullivan, Dr. Bonna Newman, and Dan Recht for valuable discussions. This work was supported by Chesonis Family Foundation and the NSF under awards CBET 0754227 and CHE-DMR-DMS 0934480. M.W. acknowledges financial support from the NSF Graduate Research Fellowship program. We acknowledge access to Shared Experimental Facilities provided by MIT Center for Materials Science Engineering supported in part by MRSEC Program of NSF under award number DMR-0213282.

References

1. M.-J. Sher, M.T. Winkler, E. Mazur, Mater. Res. Soc. Bull. **36**, 439 (2011)
2. R.O. Carlson, R.N. Hall, E.M. Pell, J. Phys. Chem. Solids **8**, 81 (1959)
3. H.R. Vydyanath, J.S. Lorenzo, F.A. Kroger, J. Appl. Phys. **49**, 5928 (1978)
4. C. Wu, C.H. Crouch, L. Zhao, J.E. Carey, R. Younkin, J.A. Levinson, E. Mazur, R.M. Farrell, P. Gothoskar, A. Karger, Appl. Phys. Lett. **78**, 1850 (2001)
5. C.H. Crouch, J.E. Carey, M. Shen, E. Mazur, F.Y. Génin, Appl. Phys. A, Mater. Sci. Process. **79**, 1635 (2004)
6. M.A. Sheehy, B.R. Tull, C.M. Friend, E. Mazur, Mater. Sci. Eng. B, Solid-State Mater. Adv. Technol. **137**, 289 (2007)
7. B.R. Tull, M.T. Winkler, E. Mazur, Appl. Phys. A, Mater. Sci. Process. **96**, 327 (2009)
8. R. Younkin, J.E. Carey, E. Mazur, J.A. Levinson, C.M. Friend, J. Appl. Phys. **93**, 2626 (2003)
9. J.E. Carey, C.H. Crouch, M. Shen, E. Mazur, Opt. Lett. **30**, 1773 (2005)
10. Alicona Imaging—MeX. http://www.alicona.com/home/products/Mex/MeX.en.php
11. C.H. Crouch, J.E. Carey, J.M. Warrender, M.J. Aziz, E. Mazur, F.Y. Genin, Appl. Phys. Lett. **84**, 1850 (2004)
12. V. Zorba, N. Boukos, I. Zergioti, C. Fotakis, Appl. Opt. **47**, 1846 (2008)
13. B.R. Tull, J.E. Carey, E. Mazur, J. McDonald, S.M. Yalisove, Mater. Res. Soc. Bull. **31**, 7 (2006)
14. A.J. Pedraza, J.D. Fowlkes, D.H. Lowndes, Appl. Phys. Lett. **74**, 2322 (1999)
15. T.E. Glover, J. Opt. Soc. Am. B **20**, 125 (2003)
16. H. Okamoto, *Desk Handbook: Phase Diagrams for Binary Alloys* (ASM International, Materials Park, 2010)
17. M.J. Smith, Y.T. Lin, M.J. Sher, M.T. Winkler, E. Mazur, S. Gradečak J. App. Phys. **110**, 053524 (2011)